1-28-2022

Measuring the thickness of vertebral endplate and shell using digital tomosynthesis

Yener N. Yeni
Henry Ford Health, YYENI1@hfhs.org

Michael R. Dix
Henry Ford Health, mdix2@hfhs.org

Angela Xiao
Henry Ford Health

Daniel J. Oravec
Henry Ford Health, DORAVEC1@hfhs.org

Michael J. Flynn
Henry Ford Health, MFLYNN1@hfhs.org

Recommended Citation
Yeni YN, Dix MR, Xiao A, Oravec DJ, and Flynn MJ. Measuring the thickness of vertebral endplate and shell using digital tomosynthesis. Bone 2022; 116341.

Bone 157 (2022) 116341

Contents lists available at ScienceDirect

Bone

journal homepage: www.elsevier.com/locate/bone

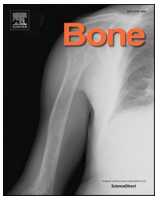

Measuring the thickness of vertebral endplate and shell using digital tomosynthesis

Yener N. Yeni [a,*], Michael R. Dix [a,b], Angela Xiao [a], Daniel J. Oravec [a], Michael J. Flynn [a]

[a] Bone and Joint Center, Henry Ford Hospital, Detroit, MI, United States of America
[b] School of Medicine, Wayne State University, Detroit, MI, United States of America

ARTICLE INFO

Keywords:
Cortical thickness
Vertebral endplate
Vertebral shell
Microcomputed tomography
Digital tomosynthesis
Bone imaging

ABSTRACT

The vertebral endplate and cortical shell play an important structural role and contribute to the overall strength of the vertebral body, are at highest risk of initial failure, and are involved in degenerative disease of the spine. The ability to accurately measure the thickness of these structures is therefore important, even if difficult due to relatively low resolution clinical imaging. We posit that digital tomosynthesis (DTS) may be a suitable imaging modality for measurement of endplate and cortical shell thickness owing to the ability to reconstruct multiplanar images with good spatial resolution at low radiation dose. In this study, for 25 cadaveric L1 vertebrae, average and standard deviation of endplate and cortical shell thickness were measured using images from DTS and microcomputed tomography (μCT). For endplate thickness measurements, significant correlations between DTS and μCT were found for all variables when comparing thicknesses measured in both the overall endplate volume (R^2 = 0.25–0.54) and when measurements were limited to a central range of coronal or sagittal slices (R^2 = 0.24–0.62). When compared to reference values from the overall shell volume, DTS thickness measurements were generally nonsignificant. However, when measurement of cortical shell thickness was limited to a range of central slices, DTS outcomes were significantly correlated with reference values for both sagittal and coronal central regions (R^2 = 0.21–0.49). DTS may therefore offer a means for measurement of endplate thickness and, within a limited sagittal or coronal measurement volume, for measurement of cortical shell thickness.

1. Introduction

Cortical shell and bony endplates, though constituting a small percentage of vertebral bone [1,2], are important structural features in vertebrae. Osteoporotic vertebral fractures often involve endplate injuries [3,4], and those with an endplate or shell fracture are more likely to progress to more severe grades [5]. Patients with vertebral fractures involving an endplate or shell injury are also more likely to develop new vertebral deformities [5].

In computational and experimental studies with cadaveric vertebrae, the endplate has been noted to undergo substantial deflection when the vertebra is compressed [6,7], and has been identified as the vertebral structure at highest risk of initial failure [8]. As in clinical vertebral fractures, compressive overload and fatigue fracture of vertebral bodies result in endplate damage in laboratory experiments [9,10]. Removal of endplates affects the load carrying capacity of the shell as well [11], and causes 33–50% reduction in vertebral stiffness and strength [12,13]. Vertebral endplate defects and fractures have also been implicated in the degenerative disease of the spine [14,15]. Specifically, endplate thickness has been correlated to local stiffness and strength at the vertebral surface [16], pressure experienced by the adjacent intervertebral disk during mechanical loading of the vertebra [17] and proteoglycan content [18] in the adjacent intervertebral disk, associated with porosity and nutrient permeability through endplate [17,19], and degeneration in the adjacent intervertebral disk [19,20].

Cortical shell has been noted to be thinner in those with osteoporosis [21] and vertebral deformities [22] as well as in women not receiving compared to those receiving hormone replacement therapy [23]. Biomechanical testing and computational studies reported that 10–63% of compressive loads are supported by the cortical shell in human vertebrae [11,24–27], and that shell thickness has been associated with work to failure independently from BMD [28]. In addition, cortical shell thickness has been associated with implant stability and strength in the spine [29,30]. As such, measurements of vertebral shell and endplate thickness could be desirable for guidance in clinical decision making.

Measurement of vertebral shell thickness using clinical CT scanners

* Corresponding author at: Bone & Joint Center, Henry Ford Hospital, Integrative Biosciences Center (iBio), 6135 Woodward, Detroit, MI 48202, USA.
E-mail address: yeni@bjc.hfh.edu (Y.N. Yeni).

https://doi.org/10.1016/j.bone.2022.116341
Received 17 June 2021; Received in revised form 7 December 2021; Accepted 23 January 2022
Available online 28 January 2022

is subject to large errors, especially for vertebrae with thin cortices, though moderate correlations could be found with reference measurements [31–34]. Recent work has shown improvement for measurement of vertebral shell [35], however measuring endplate thickness using CT remains especially difficult, as the direction for measuring endplate thickness is also the direction of poorest resolution in CT scans. Digital tomosynthesis (DTS) is a clinically available imaging modality with potential to measure vertebral cortical thickness. It is a linear cone beam tomography system in which the x-ray source and detector move in parallel paths but opposite directions to produce sharply focused planes with 2.41–3.16 times better resolution than current CT systems [36,37]. Unlike plain radiography, DTS allows for an analysis of the object at a depth of interest with less visual clutter from the rest of the object. In addition, the radiation dose for DTS examination of the spine is 12–17% that of a typical CT dose [38,39]. It has been shown that DTS can quantify the surface topography of vertebral endplates [40]; however, the extent to which DTS can quantify vertebral shell and endplate thickness is unknown. Therefore, the objective of the current study was to examine the ability of DTS to measure human vertebral shell and endplate thickness with microcomputed tomography (μCT) as a reference.

2. Methods

All the procedures including acquisition of cadaveric materials were performed under the approval of the Institutional Review Board (IRB). Human cadaveric spines were acquired from national tissue donation programs (the National Disease Research Interchange (NDRI, Philadelphia, PA) and Biological Resource Center (BRC, Phoenix, AZ)). Lumbar 1 vertebrae were harvested under local IRB approval from 25 donors (14 Males, 11 Females; 41–100 years age). Donors with a history of HIV, hepatitis, diabetes, renal failure, metastatic cancer, osteomalacia, hyperparathyroidism, Paget's disease of bone, spine surgery, cause of death involving trauma, and corticosteroid, anticonvulsant or bisphosphonate use were not included, either due to safety concerns or known effects of these conditions on bone metabolism.

Specimens were dissected, cleaned of soft tissue, posterior elements were removed, then imaged using μCT and DTS. Microcomputed tomography imaging was performed using a custom-built μCT system and reconstructed at 40 μm voxel size using parameters described previously [41]. At the time of μCT imaging, we noted any endplate abnormalities. Although some specimens had Schmorl's nodes, there were no specimens with notable osteophytes. The images were analyzed as-is for both reference and experimental modalities, so all endplate and shell features were taken into account in the correlations. DTS imaging was performed on a clinical imaging system (Shimadzu Sonialvision Saffire II) with specimens mounted in a custom, sealed radiolucent tank filled with 0.9% saline. DTS imaging was performed using a standard clinical spine protocol in both AP (producing a reconstructed stack of coronal plane images with 0.279 × 0.279 mm pixels and slice thickness of 1 mm) and LM (producing a stack of sagittal plane images with 0.279 × 0.279 mm pixels and slice thickness of 1 mm) orientations while aligned axially (0°) or transversely (90°) to the superior-inferior axis of the vertebrae [40,42].

Axially oriented DTS images were used for analysis of endplate thickness and transversely oriented images were used for analysis of shell thickness, to account for the effect of scanning direction on the ability to resolve structures oriented parallel or perpendicular to the tomosynthesis sweep direction [42]. A global threshold was applied to delineate bone from soft tissue in DTS images [40]. Volumes comprising the endplate and cortical shell were cropped from the binarized images (Figs. 1-2). μCT images were segmented using the workflow described previously [40]. In short, the first stage of segmentation is focused on masking the exterior surface without affecting the center of the vertebra. To this end, a specimen specific, temporary threshold value which delineates the periosteal boundary is manually determined for each specimen. This threshold value is applied temporarily, after which rays are directed at each voxel from 26 directions [43]. If the ray is incident on the voxel from 2 or more of the 26 directions, that voxel is considered to be outside the vertebral surface. The resulting volume is again thresholded at the soft tissue value to delineate the endosteal surface. The resulting masks ("shell" and "void") produced by these procedures are further processed with a series of morphological closing operations [44] to produce closed surface masks of each compartment. The two

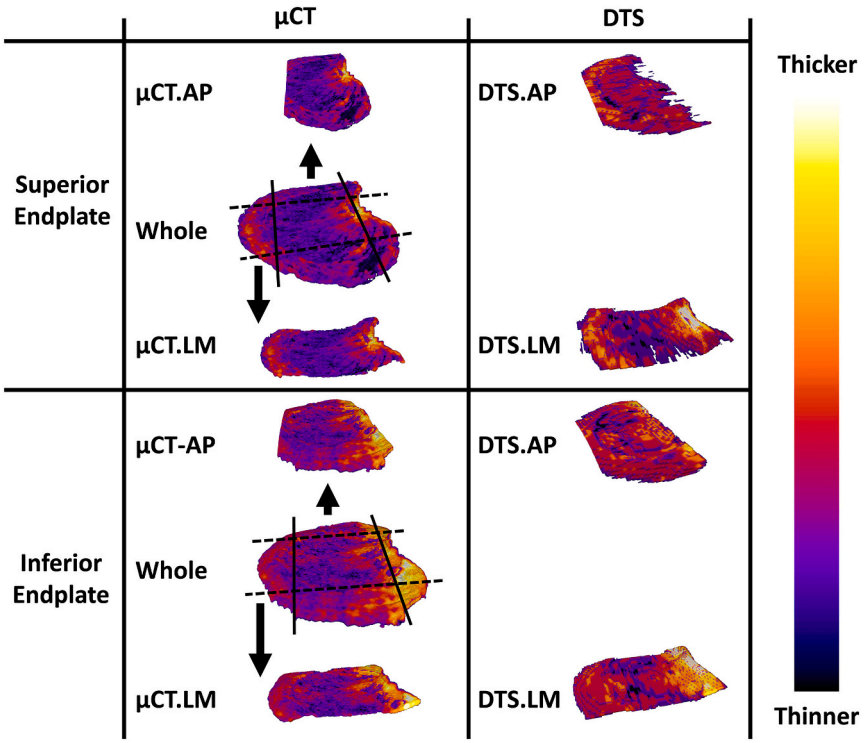

Fig. 1. Representation of endplate analysis volumes from μCT and DTS. DTS was first correlated with μCT (whole). As an alternative approach, regions (.AP and .LM) were created from μCT to match the central 25 mm DTS analysis region. Endplate thickness distributions (color coded from minimum to maximum thickness within each analyzed region) are overlaid for a L1 vertebra from a 74 year old male. (For interpretation of the references to color in this figure legend, the reader is referred to the web version of this article.)

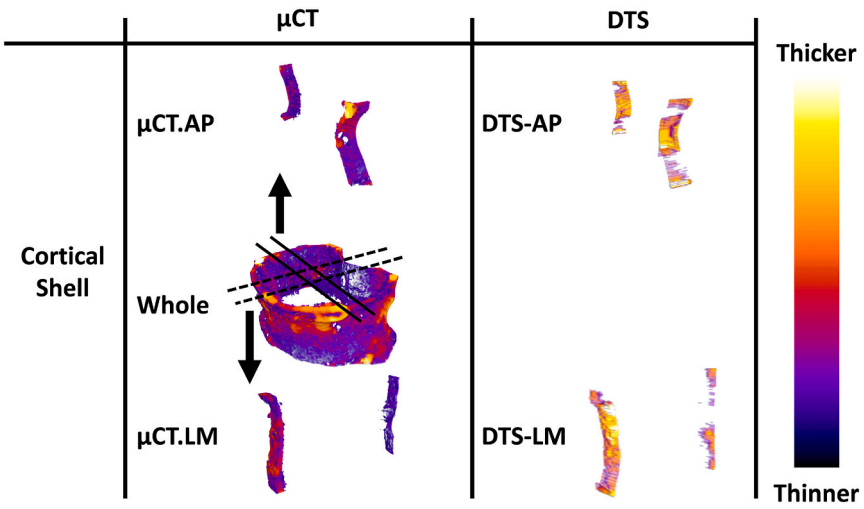

Fig. 2. Representation of cortical shell analysis volumes from μCT and DTS. DTS was first correlated with μCT (whole). As an alternative approach, regions (.AP and .LM) were created from μCT to match the central 6 mm DTS analysis region. Cortical shell thickness distributions (color coded from minimum to maximum thickness within each analyzed region) are overlaid for a L1 vertebra from a 70 year old female. (For interpretation of the references to color in this figure legend, the reader is referred to the web version of this article.)

compartments are multiplied using image arithmetic to separate the cortical compartment (shell and endplate) from cancellous bone and background. For μCT images, local thickness was measured at each voxel using a 3D local sphere-fitting algorithm in ImageJ. A 2D, slice-by-slice implementation (local circle-fitting) was applied to DTS images [45]. Cropping regions and representative thickness distributions from endplate and shell analyses are illustrated in Figs. 1 and 2.

For DTS images, the endplate volume of interest was defined as a central slab of 25 mm width in both AP (i.e., excluding lateral cortices) and LM (i.e., excluding anterior and posterior cortices) views to avoid blurring artifacts from the end slices of the image stack. The DTS volume of interest for cortical shell analysis was defined as a central slab of 6 mm width in AP and LM views. As an alternative approach for defining analysis regions in μCT images, rather than using the entire shell and endplate volumes, a central volume was extracted to match the DTS volume of interest. In this approach, volumes of interest for μCT were also defined as a central slab of 25 mm width (for endplate analyses) or 6 mm width (for cortical shell analyses) in both AP and LM directions as described above for DTS (Figs. 1-2).

Average thickness was calculated for superior and inferior endplates (EP.Th.S.Av and EP.Th.I.Av), and the shell (Sh.Th.Av) from each imaging modality. Standard deviation of the thickness distribution within a specimen was also calculated as a measure of thickness heterogeneity (EP.Th.S.SD, EP.Th.I.SD and Sh.Th.SD) as this was suggested to be a useful metric in previous reports [33,46].

The differences and the relationships between DTS- and μCT-derived thickness variables were examined using matched pairs and regression analyses in JMP (v10, SAS Institute Inc., Cary, NC). Statistical significance was considered as $p < 0.05$.

3. Results

Based on μCT measurements, inferior and superior endplates as well as cortical shell in the AP-matched and LM-matched central slabs were all thinner than those in the whole volume (4.5% to 10.1% for endplate and 7.3%–21.2% for shell measurements, $p = 0.065$ to $p < 0.0001$). AP-matched central slabs were also thinner than LM-matched central slabs, albeit marginally significant ($p = 0.052$). Endplate and shell thickness results are summarized by modality with the average and standard deviation of measurements, as well as mean error and standard error of mean differences from μCT for the whole vertebral (Table 1a) and matched central volumes (Table 1b). When whole volumes were considered, statistically significant differences between DTS and reference measurements were observed for average (9.4–21.7%) and standard deviation of thicknesses (18.2–35.2%) (Table 1a). When matched volumes were considered, differences between DTS and reference measurements were generally smaller (0.71–16%). For matched volumes, differences were no longer statistically significant for average thickness measured at the inferior endplate (2.8–4.8%) ($p > 0.05$ for both AP and LM views). Similarly, differences were no longer significant for both average and standard deviation of shell thickness from LM images (0.71% and 22.7%, respectively) (Table 1b).

Table 1a
The average (Av) and heterogeneity (SD) of endplate and shell thickness values by modality within the whole volume: Mean ± Standard deviation (Mean difference from μCT ± Standard error of difference) (mm).

		μCT	DTS.AP	DTS.LM
Inferior endplate	Av	0.672 ± 0.156	0.606 ± 0.116 (−0.066 ± 0.023) $p < 0.01$	0.609 ± 0.098 (−0.063 ± 0.023) $p < 0.02$
	SD	0.306 ± 0.085	0.229 ± 0.062 (−0.077 ± 0.013) $p < 0.0001$	0.243 ± 0.061 (−0.063 ± 0.012) $p < 0.0001$
Superior endplate	Av	0.728 ± 0.156	0.592 ± 0.094 (−0.136 ± 0.024) $p < 0.0001$	0.570 ± 0.071 (−0.159 ± 0.025) $p < 0.0001$
	SD	0.350 ± 0.113	0.226 ± 0.062 (−0.124 ± 0.019) $p < 0.0001$	0.224 ± 0.040 (−0.125 ± 0.020) $p < 0.0001$
Shell	Av	0.715 ± 0.171	0.582 ± 0.075 (−0.134 ± 0.033) $p < 0.0006$	0.568 ± 0.090 (−0.148 ± 0.026) $p < 0.0001$
	SD	0.371 ± 0.127	0.191 ± 0.042 (−0.180 ± 0.025) $p < 0.0001$	0.204 ± 0.056 (−0.168 ± 0.024) $p < 0.0001$

All DTS endplate thickness measurements were significantly correlated to the corresponding measurements from μCT when the whole volume was considered ($R^2 = 0.25$ to 0.54; $p < 0.02$ to $p < 0.0001$) (Table 2, Fig. 3). For significant relationships, the slope estimates were close to 1 (0.903 to 1.419) with nonsignificant intercepts (Table 2, Fig. 3). Average shell thickness correlated to μCT for the LM view only ($R^2 = 0.42$; $p < 0.0005$) (Table 2, Fig. 4).

When the correlations were examined within a matched central slab volume, rather than the whole volume, all correlations between μCT- and DTS-derived variables were still significant for the endplate (Table 3). Within the matched volumes, correlations of Sh.Th.Av and Sh.

Table 1b
The average (Av) and heterogeneity (SD) of endplate and shell thickness values by modality within the central slabs: Mean ± Standard deviation (Mean difference from μCT ± Standard error of difference) (mm).

		μCT-AP	μCT-LM	DTS.AP	DTS.LM
Inferior endplate	Av	0.642 ± 0.146	0.632 ± 0.147	0.611 ± 0.113 (−0.031 ± 0.022) $p > 0.1$	0.614 ± 0.097 (−0.017 ± 0.020) $p > 0.4$
	SD	0.295 ± 0.083	0.302 ± 0.083	0.233 ± 0.064 (−0.063 ± 0.013) $p < 0.0001$	0.247 ± 0.064 (−0.055 ± 0.010) $p < 0.0001$
Superior endplate	Av	0.701 ± 0.150	0.655 ± 0.126	0.589 ± 0.099 (−0.112 ± 0.022) $p < 0.0001$	0.578 ± 0.077 (−0.077 ± 0.022) $p < 0.003$
	SD	0.347 ± 0.119	0.308 ± 0.074	0.225 ± 0.067 (−0.123 ± 0.019) $p < 0.0001$	0.226 ± 0.043 (−0.082 ± 0.013) $p < 0.0001$
Shell	Av	0.663 ± 0.186	0.564 ± 0.250	0.582 ± 0.075 (−0.082 ± 0.033) $p < 0.02$	0.568 ± 0.090 (0.004 ± 0.039) $p > 0.9$
	SD	0.255 ± 0.128	0.264 ± 0.201	0.191 ± 0.042 (−0.064 ± 0.023) $p < 0.02$	0.204 ± 0.056 (−0.060 ± 0.034) $p > 0.09$

Th.SD from DTS with those from μCT were also significant for both AP and LM views ($p < 0.02$ to $p < 0.0001$) (Table 3).

4. Discussion

We examined the extent to which digital tomosynthesis imaging can be utilized for measurement of vertebral endplate and shell thickness, with μCT as the reference modality using cadaveric vertebrae. We found moderate correlations between DTS and μCT with R^2 values ranging from 0.24 to 0.62.

Our reference endplate measurements (Table 1a, Table 1b) are generally in agreement with results from previous studies that used μCT or microscopy and examined L1 vertebrae [10,16,20,47]. We did not attempt to categorize the endplate as single- or double-layer [48], as this would typically require high resolution that would prohibit imaging of the entire vertebral body in our μCT system. Some studies reported a minimum and maximum endplate thickness at a given location, without specifically labeling the endplate as single- or double-layer [31,49], and our results appear to be in better agreement with those reported as the maximum thickness. Reference values for cortical shell similarly appear to be within the range of literature values for L1 vertebrae, though they better agree with higher values within the range (0.09–1.18) [16,21,31,49,50].

DTS endplate and shell thickness measurements were generally in the vicinity of, though somewhat lower than, μCT reference values. There is unfortunately no point of comparison in the literature for DTS endplate or shell thickness. On average, thickness values were 9.4–21.7% lower than reference values for the whole volume (Table 1a). This difference was even lower when matched volumes were considered (0.7–15%, Table 1b). The overall magnitude in bias is considerably smaller than previous studies using clinical CT [22,31,34], and is similar to best results achieved using advanced computational methods comparing HR-QCT to HR-pQCT (19% overestimation, [35]). In these applications, CT appears useful for measurement of shell thickness [22,23,34,35], however measuring endplate thickness is particularly difficult using CT and typically overestimated [16,31,51], as it is measured in the direction of poorest resolution. DTS endplate thickness measurements are performed within the planes of highest resolution and, despite scatter around regression lines resulting in moderate R^2 values, demonstrated slopes close to 1. Though DTS endplate thickness was only moderately correlated to reference measurements, the finding is significant as it offers the capacity, even if in a limited fashion, for clinical studies addressing vertebral endplate.

Average shell thickness measured from DTS was correlated with μCT for the LM view only, and Sh.Th.SD was not correlated with μCT when the entire reference volume was utilized for correlation (Table 2). However, when the reference analysis volume was limited to a central

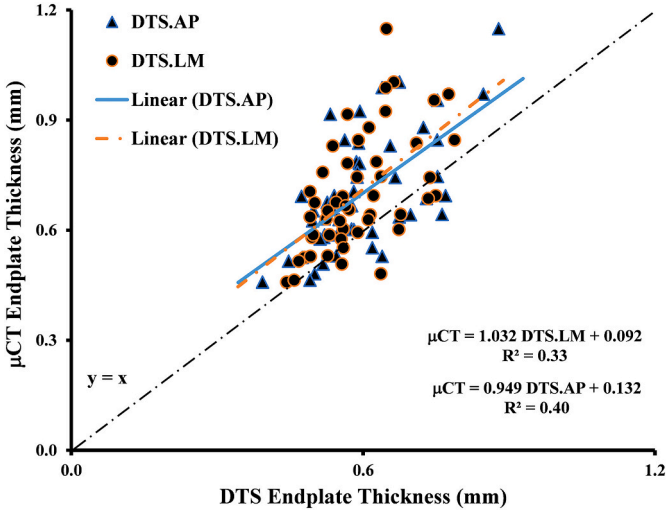

Fig. 3. EP.Th measured from μCT vs DTS. EP.Th from superior and inferior endplates were pooled for this plot.

Table 2
Results for linear regression between cortical thickness variables measured from DTS (AP and LM) and μCT. NS = nonsignificant.

		Inferior EP		Superior EP		Shell	
		μCT.Av	μCT.SD	μCT.Av	μCT.SD	μCT.Av	μCT.SD
DTS.AP	R^2	0.45	0.45	0.42	0.30	0.08	0.04
	Std Err	0.115	0.063	0.119	0.094	0.164	0.124
	Slope	0.903	0.916	1.077	1.008	NS	NS
	p_{sl}	<0.0002	<0.0003	<0.0005	<0.005		
	Intercept	NS	NS	NS	NS		
DTS.LM	R^2	0.47	0.54	0.36	0.25	0.42	0.11
	Std Err	0.113	0.058	0.125	0.098	0.130	0.119
	Slope	1.089	1.032	1.309	1.419	1.223	NS
	p_{sl}	<0.0001	<0.0001	<0.002	$p < 0.02$	<0.0005	
	Intercept	NS	NS	NS	NS	NS	

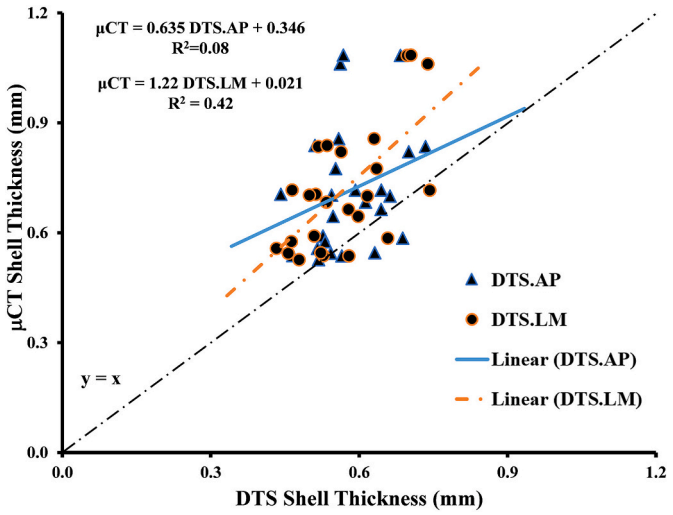

Fig. 4. Sh.Th measured from μCT vs DTS.

slab in a comparable way to DTS, the shell measurements were moderately correlated for both coronal and sagittal slabs (Table 3). The correlation between DTS and the μCT reference for matched volumes support use of DTS for shell thickness measurements in central slab of a vertebra. However, the lack of correlation for the whole volume indicates that the regions excluded by DTS are different enough from the overall shell volume that central slab measurements should not be extrapolated to the peripheries of the vertebral volume. Consideration to a central slab is not so unusual, as these types of measurements are often performed at selected sections even in X-ray tomography applications [22,31,34]. The clinical significance of cortical thickness measurement at central planes within the vertebral body has been well established through histological studies analyzing these very regions. For example, Ritzel et al. found that decreased cortical shell thickness within relatively thin (4 mm) central sections was significantly associated with age and osteoporosis [21]. In terms of biomechanical significance, cortical shell thickness measured at central regions has been shown to be a major determinant of mechanical strength and work to failure [28,52]. Changes in endplate central regions may also affect nutrient supply, leading to localized loss of proteoglycan in the adjacent nucleus [18,53]. Taken together, analysis of central regions is well supported in terms of biomechanical changes due to structural changes resulting from aging and disease.

Given the moderate level of correlations, measurement error is certainly an issue in terms of clinical utility of these methods. There is no established clinical practice utilizing EP or shell thickness, so the tolerable amount of error is unknown. However, biologically, biomechanically and clinically significant observations have been made in EP and shell thickness. Approximately 50% decrease in EP thickness [18] and 32% decrease in shell thickness [21] have been noted from 30 to 80 years of age, suggesting measurable variations in EP thickness may have age-related significance. In biomechanical studies, % changes in EP and shell thicknesses corresponded to comparable % changes in EP stiffness and adjacent disc pressure [16], and stability of a vertebral implant [29]. According to Ritzel et al., cortical thickness decreases due to osteoporosis may be on the order of 15–30%, and differences in shell thickness as low as 6% to 16.7% that were associated with vertebral deformity [22] or hormone replacement therapy [23] were detectable using clinical CT scanners. These small differences were detectable using images from clinical resolution CT scanners and approximating the vertebral body to a cylinder. We expect direct measurements of thickness from DTS images may be similarly used to separate clinically significant groups, although the acceptable level of error is likely application specific. In future work with larger sample sizes, it may be possible to establish confidence intervals to help more precisely define the clinical utility of these measurements.

This study is not without limitations. The findings of this study are limited to the L1 vertebral level. However, L1 is clinically relevant as it is one of the most common sites of osteoporotic fractures [54]. The L1 level also has the thinnest cortical shell among the lumbar vertebral levels [10,21], so the current results likely represent a worst case scenario for the entire lumbar spine. Future work will extend the findings of the current study to other vertebral levels. In addition, image pre-processing methods obviously have considerable bearing on thickness measurements, and the sphere fitting approach implemented in the current work is dependent on the quality of segmentation. Although the thresholding methods produced visually acceptable results and were applied uniformly, it is possible that alternative image pre-processing schemes (e.g., adaptive thresholding, local contrast enhancement, or other filtration) may increase accuracy of the solutions. Also, in an effort to minimize image pre-processing and to constrain the measurement within the highest resolution planes, reconstructed DTS images were not resampled prior to the calculation and a slice-by-slice circle-fitting approach was applied to the series of 2D planes. However, it may be possible to further improve DTS endplate thickness correlations by considering resampling the gray volumes to isotropic voxel size prior to binarization and performing a 3D calculation. It should also be noted that a comparison with CT imaging was not included in the current study. More recently, computational approaches for thickness measurement using machine learning [55,56] and radial gray value profiles [35] have shown promise in the CT literature, the latter being particularly promising for CT images of vertebral shell [35], however these techniques have not been established for vertebral endplate. Upon examination of these image processing methods, a more informative comparison would be possible in future work.

In conclusion, this is the first study attempting to use DTS for cortical thickness measurements in vertebrae. The results indicate that DTS may

Table 3
Results for linear regression between cortical thickness variables measured from DTS (AP and LM) and μCT using matching image volumes. NS = nonsignificant.

		Inferior EP		Superior EP		Shell	
		μCT.Av	μCT.SD	μCT.Av	μCT.SD	μCT.Av	μCT.SD
DTS.AP	R^2	0.42	0.41	0.48	0.39	0.23	0.21
	Std Err	0.111	0.064	0.108	0.092	0.163	0.114
	Slope	0.837	0.830	1.058	1.112	1.184	1.391
	p_{sl}	<0.0004	<0.0006	<0.0001	<0.0008	<0.02	<0.03
	Intercept p_{int}	NS	NS	NS	NS	NS	NS
DTS.LM	R^2	0.53	0.62	0.24	0.28	0.49	0.38
	Std Err	0.101	0.051	0.110	0.063	0.178	0.158
	Slope	1.112	1.029	0.791	0.904	1.944	2.220
	p_{sl}	<0.0001	<0.0001	<0.02	<0.007	<0.0001	<0.001
	Intercept p_{int}	NS	NS	NS	NS	−0.540 <0.04	NS

offer a means for measuring endplate and cortical shell. Future work is needed to explore the possibility of increasing the precision of the measurements by further optimizing planes of view, analysis volumes and image processing approaches.

CRediT authorship contribution statement

Yener N. Yeni: Conceptualization, Formal analysis, Resources, Writing – original draft, Visualization, Project administration, Funding acquisition. **Michael R. Dix:** Software, Investigation, Formal analysis, Writing – review & editing. **Angela Xiao:** Investigation, Formal analysis, Writing – review & editing. **Daniel J. Oravec:** Methodology, Software, Formal analysis, Investigation, Writing – original draft, Visualization, Supervision. **Michael J. Flynn:** Conceptualization, Methodology, Resources, Project administration.

Declaration of competing interest

None.

Acknowledgements

This project was supported, in part, by the National Institutes of Health under NIH grant AR059329. Its contents are solely the responsibility of the authors and do not necessarily represent the official views of NIH. We thank Nicole Ramo for her help with specimen dissection and image processing. We acknowledge use of human tissues provided by National Disease Research Interchange (NDRI) and Biological Resource Center (BRC).

References

[1] S.K. Eswaran, H.H. Bayraktar, M.F. Adams, A. Gupta, P.F. Hoffmann, D.C. Lee, P. Papadopoulos, T.M. Keaveny, The micro-mechanics of cortical shell removal in the human vertebral body, Comput. Methods Appl. Mech. Eng. 196 (31–32) (2007) 3025–3032.
[2] R. Eastell, L. Mosekilde, S.F. Hodgson, B.L. Riggs, Proportion of human vertebral body bone that is cancellous, J. Bone Miner. Res. 5 (12) (1990) 1237–1241.
[3] T. Fujiwara, K. Akeda, J. Yamada, T. Kondo, A. Sudo, Endplate and intervertebral disc injuries in acute and single level osteoporotic vertebral fractures: is there any association with the process of bone healing? BMC Musculoskelet. Disord. 20 (1) (2019) 336.
[4] A.O. Ortiz, R. Bordia, Injury to the vertebral endplate-disk complex associated with osteoporotic vertebral compression fractures, AJNR Am. J. Neuroradiol. 32 (1) (2011) 115–120.
[5] Y.X.J. Wang, N. Che-Nordin, M. Deng, J.C.S. Leung, A.W.L. Kwok, L.C. He, J. F. Griffith, T.C.Y. Kwok, P.C. Leung, Osteoporotic vertebral deformity with endplate/cortex fracture is associated with higher further vertebral fracture risk: the Ms. OS (Hong Kong) study results, Osteoporos. Int. 30 (4) (2019) 897–905.
[6] T.M. Jackman, A.I. Hussein, A.M. Adams, K.K. Makhnejia, E.F. Morgan, Endplate deflection is a defining feature of vertebral fracture and is associated with properties of the underlying trabecular bone, J. Orthop. Res. 32 (7) (2014) 880–886.
[7] P. Brinckmann, W. Frobin, E. Hierholzer, M. Horst, Deformation of the vertebral end-plate under axial loading of the spine, Spine 8 (8) (1983) 851–856.
[8] S.K. Eswaran, A. Gupta, T.M. Keaveny, Locations of bone tissue at high risk of initial failure during compressive loading of the human vertebral body, Bone 41 (4) (2007) 733–739.
[9] T. Hansson, T. Keller, R. Jonson, Fatigue fracture morphology in human lumbar motion segments, J. Spinal Disord. 1 (1) (1988) 33–38.
[10] P. Dolan, J. Luo, P. Pollintine, P.R. Landham, M. Stefanakis, M.A. Adams, Intervertebral disc decompression following endplate damage: implications for disc degeneration depend on spinal level and age, Spine 38 (17) (2013) 1473–1481.
[11] S.K. Eswaran, A. Gupta, M.F. Adams, T.M. Keaveny, Cortical and trabecular load sharing in the human vertebral body, J. Bone Miner. Res. 21 (2) (2006) 307–314.
[12] Y. Hou, W. Yuan, J. Kang, Y. Liu, Influences of endplate removal and bone mineral density on the biomechanical properties of lumbar spine, PloS one 8 (11) (2013), e76843.
[13] T.R. Oxland, J.P. Grant, M.F. Dvorak, C.G. Fisher, Effects of endplate removal on the structural properties of the lower lumbar vertebral bodies, Spine 28 (8) (2003) 771–777.
[14] Y. Wang, T. Videman, M.C. Battie, ISSLS prize winner: lumbar vertebral endplate lesions: associations with disc degeneration and back pain history, Spine 37 (17) (2012) 1490–1496.
[15] A. Przybyla, P. Pollintine, R. Bedzinski, M.A. Adams, Outer annulus tears have less effect than endplate fracture on stress distributions inside intervertebral discs: relevance to disc degeneration, Clin. Biomech. (Bristol, Avon) 21 (10) (2006) 1013–1019.
[16] A. Noshchenko, A. Plaseied, V.V. Patel, E. Burger, T. Baldini, L. Yun, Correlation of vertebral strength topography with 3-dimensional computed tomographic structure, Spine 38 (4) (2013) 339–349.
[17] U. Zehra, K. Robson-Brown, M.A. Adams, P. Dolan, Porosity and thickness of the vertebral endplate depend on local mechanical loading, Spine 40 (15) (2015) 1173–1180.
[18] S. Roberts, I.W. McCall, J. Menage, M.J. Haddaway, S.M. Eisenstein, Does the thickness of the vertebral subchondral bone reflect the composition of the intervertebral disc? Eur. Spine J. 6 (6) (1997) 385–389.
[19] A.G. Rodriguez, A.E. Rodriguez-Soto, A.J. Burghardt, S. Berven, S. Majumdar, J. C. Lotz, Morphology of the human vertebral endplate, J. Orthop. Res. 30 (2) (2012) 280–287.
[20] Y. Wang, M.C. Battié, S.K. Boyd, T. Videman, The osseous endplates in lumbar vertebrae: thickness, bone mineral density and their associations with age and disk degeneration, Bone 48 (4) (2011) 804–809.
[21] H. Ritzel, M. Amling, M. Pösl, M. Hahn, G. Delling, The thickness of human vertebral cortical bone and its changes in aging and osteoporosis: a histomorphometric analysis of the complete spinal column from thirty-seven autopsy specimens, J. Bone Miner. Res. 12 (1) (1997) 89–95.
[22] L.J. Melton 3rd, B.L. Riggs, T.M. Keaveny, S.J. Achenbach, D. Kopperdahl, J. J. Camp, P.A. Rouleau, S. Amin, E.J. Atkinson, R.A. Robb, T.M. Therneau, S. Khosla, Relation of vertebral deformities to bone density, structure, and strength, J. Bone Miner. Res. 25 (9) (2010) 1922–1930.
[23] P. Eser, J. Cook, J. Black, R. Iles, R. Daly, R. Ptasznik, S. Bass, Interaction between playing golf and HRT on vertebral bone properties in post-menopausal women measured by QCT, Osteoporos. Int. 19 (3) (2008) 311–319.
[24] J. Homminga, H. Weinans, W. Gowin, D. Felsenberg, R. Huiskes, Osteoporosis changes the amount of vertebral trabecular bone at risk of fracture but not the vertebral load distribution, Spine 26 (14) (2001) 1555–1561.
[25] K.D. Cao, M.J. Grimm, K.H. Yang, Load sharing within a human lumbar vertebral body using the finite element method, Spine 26 (12) (2001) E253–E260.
[26] M.J. Silva, T.M. Keaveny, W.C. Hayes, Load sharing between the shell and centrum in the lumbar vertebral body, Spine 22 (2) (1997) 140–150.
[27] R.J. McBroom, W.C. Hayes, W.T. Edwards, R.P. Goldberg, A.A. White 3rd, Prediction of vertebral body compressive fracture using quantitative computed tomography, J. Bone Joint Surg. Am. 67 (8) (1985) 1206–1214.
[28] J.P. Roux, J. Wegrzyn, M.E. Arlot, O. Guyen, P.D. Delmas, R. Chapurlat, M. L. Bouxsein, Contribution of trabecular and cortical components to biomechanical behavior of human vertebrae: an ex vivo study, J. Bone Miner. Res. 25 (2) (2010) 356–361.
[29] D. Ruffoni, A.J. Wirth, J.A. Steiner, I.H. Parkinson, R. Müller, G.H. van Lenthe, The different contributions of cortical and trabecular bone to implant anchorage in a human vertebra, Bone 50 (3) (2012) 733–738.
[30] Q.H. Zhang, S.H. Tan, S.M. Chou, Effects of bone materials on the screw pull-out strength in human spine, Med. Eng. Phys. 28 (8) (2006) 795–801.
[31] M. Silva, C. Wang, T. Keaveny, W. Hayes, Direct and computed tomography thickness measurements of the human, lumbar vertebral shell and endplate, Bone 15 (4) (1994) 409–414.
[32] T.N. Hangartner, V. Gilsanz, Evaluation of cortical bone by computed tomography, J. Bone Miner. Res. 11 (10) (1996) 1518–1525.
[33] G. Dougherty, D. Newman, Measurement of thickness and density of thin structures by computed tomography: a simulation study, Med. Phys. 26 (7) (1999) 1341–1348.
[34] S. Zhou, I. McCarthy, A. McGregor, R. Coombs, S. Hughes, Geometrical dimensions of the lower lumbar vertebrae–analysis of data from digitised CT images, Eur. Spine J. 9 (3) (2000) 242–248.
[35] T. Damm, J.A. Peña, G.M. Campbell, J. Bastgen, R. Barkmann, C.-C. Glüer, Improved accuracy in the assessment of vertebral cortical thickness by quantitative computed tomography using the Iterative Convolution OptimizatioN (ICON) method, Bone 120 (2019) 194–203.
[36] J.T. Dobbins 3rd, D.J. Godfrey, Digital X-ray tomosynthesis: current state of the art and clinical potential, Phys. Med. Biol. 48 (19) (2003) R65–R106.
[37] M.J. Flynn, R. McGee, J. Blechinger, Spatial Resolution of X-ray Tomosynthesis in Relation to Computed Tomography for Coronal/Sagittal Images of the Knee, SPIE, San Diego, CA, United States, 2007, pp. 65100D-9.
[38] F.A. Mettler Jr., W. Huda, T.T. Yoshizumi, M. Mahesh, Effective doses in radiology and diagnostic nuclear medicine: a catalog, Radiology 248 (1) (2008) 254–263.
[39] Y. Zhang, X. Li, W.Paul Segars, E. Samei, Comparative Dosimetry of Radiography, Tomosynthesis, And CT for Chest Imaging Across 59 Adult Patients, SPIE, Lake Buena Vista, FL, United States, The Society of Photo-Optical Instrumentation Engineers (SPIE); Aeroflex Incorporated; CREOL - Univ. Central Florida, Coll. Opt. Photonics; DQE Instruments, Inc.; Medtronic, Inc.; PIXELTEQ, Multispectral Sensing and Imaging, 2013 pp.
[40] D. Oravec, A. Quazi, A. Xiao, E. Yang, R. Zauel, M.J. Flynn, Y.N. Yeni, Digital tomosynthesis and high resolution computed tomography as clinical tools for vertebral endplate topography measurements: comparison with microcomputed tomography, Bone 81 (2015) 300–305.
[41] W. Kim, D. Oravec, S. Nekkanty, J. Yerramshetty, E.A. Sander, G.W. Divine, M. J. Flynn, Y.N. Yeni, Digital tomosynthesis (DTS) for quantitative assessment of trabecular microstructure in human vertebral bone, Med. Eng. Phys. 37 (1) (2015) 109–120.
[42] W. Kim, D. Oravec, G.W. Divine, M.J. Flynn, Y.N. Yeni, Effect of view, scan orientation and analysis volume on digital tomosynthesis (DTS) based textural analysis of bone, Ann. Biomed. Eng. 45 (5) (2017) 1236–1246.

[43] R. Zauel, D.P. Fyhrie, Y.N. Yeni, Segmentation algorithm with improved connectivity for accurate 3D representation of microcomputed tomographic images of human vertebral bodies, in: 51st Annual Meeting of the Orthopaedic Research Society, Washington, D.C, 2005, p. 1260.
[44] H.R. Buie, G.M. Campbell, R.J. Klinck, J.A. MacNeil, S.K. Boyd, Automatic segmentation of cortical and trabecular compartments based on a dual threshold technique for in vivo micro-CT bone analysis, Bone 41 (4) (2007) 505–515.
[45] R.P. Dougherty, K.-H. Kunzelmann, Computing local thickness of 3D structures with ImageJ, Microsc. Microanal. 13 (S02) (2007) 1678–1679.
[46] G. Dougherty, The peak CT number of profiles perpendicular to the vertebral cortical shell may be a useful indicator of the integrity of the cortical shell, Med. Eng. Phys. 22 (7) (2000) 487–491.
[47] P.A. Hulme, S.K. Boyd, S.J. Ferguson, Regional variation in vertebral bone morphology and its contribution to vertebral fracture strength, Bone 41 (6) (2007) 946–957.
[48] A.J. Fields, F.S. Costabal, A.G. Rodriguez, J.C. Lotz, Seeing double: a comparison of microstructure, biomechanical function, and adjacent disc health between double-layer and single-layer vertebral endplates, Spine 37 (21) (2012) E1310.
[49] W.T. Edwards, Y. Zheng, L.A. Ferrara, H.A. Yuan, Structural features and thickness of the vertebral cortex in the thoracolumbar spine, Spine 26 (2) (2001) 218–225.
[50] V. Palepu, S.D. Rayaprolu, S. Nagaraja, Differences in trabecular bone, cortical shell, and endplate microstructure across the lumbar spine, Int.J.Spine Surg. 13 (4) (2019) 361–370.
[51] T. Pitzen, B. Schmitz, T. Georg, D. Barbier, T. Beuter, W.I. Steudel, W. Reith, Variation of endplate thickness in the cervical spine, Eur. Spine J. 13 (3) (2004) 235–240.
[52] A. Vesterby, L. Mosekilde, H. Gundersen, F. Melsen, L. Mosekilde, K. Holme, S. Sørensen, A. Bone, M.R. Group, Biologically meaningful determinants of the in vitro strength of lumbar vertebrae, Bone 12 (3) (1991) 219–224.
[53] D.M. Soukane, A. Shirazi-Adl, J. Urban, Computation of coupled diffusion of oxygen, glucose and lactic acid in an intervertebral disc, J. Biomech. 40 (12) (2007) 2645–2654.
[54] M. Van der Klift, C.E. De Laet, E.V. McCloskey, A. Hofman, H.A. Pols, The incidence of vertebral fractures in men and women: the Rotterdam Study, J. Bone Miner. Res. 17 (6) (2002) 1051–1056.
[55] L. Humbert, J. Hazrati Marangalou, L.M. del Río Barquero, G.H. van Lenthe, B. van Rietbergen, Cortical thickness and density estimation from clinical CT using a prior thickness-density relationship, Med. Phys. 43 (4) (2016) 1945–1954.
[56] V. Chandran, G. Maquer, T. Gerig, P. Zysset, M. Reyes, Supervised learning for bone shape and cortical thickness estimation from CT images for finite element analysis, Med. Image Anal. 52 (2019) 42–55.